Field-induced single-ion magnet performing tri-axial anisotropy in an 1D Co(II) coordination polymer with rigid linker ligand 4,4'-(buta-1,3-diyne-1,4-diyl)dibenzoate

Catiúcia R. M. O. Matos,[a] Charlie V. Sarmiento,[b] Henrique C. Silva Jr,[a] Glaucio B. Ferreira,[a] Guilherme P. Guedes,[a] Wallace C. Nunes,[b] and Célia M. Ronconi[,a]*

[a]*Departamento de Química Inorgânica, Universidade Federal Fluminense (UFF), Outeiro de São João Batista, s/n, Campus do Valonguinho, Centro, 24020-141, Niterói, RJ, Brazil*

[b]*Instituto de Física, Universidade Federal Fluminense (UFF), Niterói-RJ, 24210-271, Brazil*

Corresponding authors: cmronconi@id.uff.br

Electronic Supporting Information

Table of contents

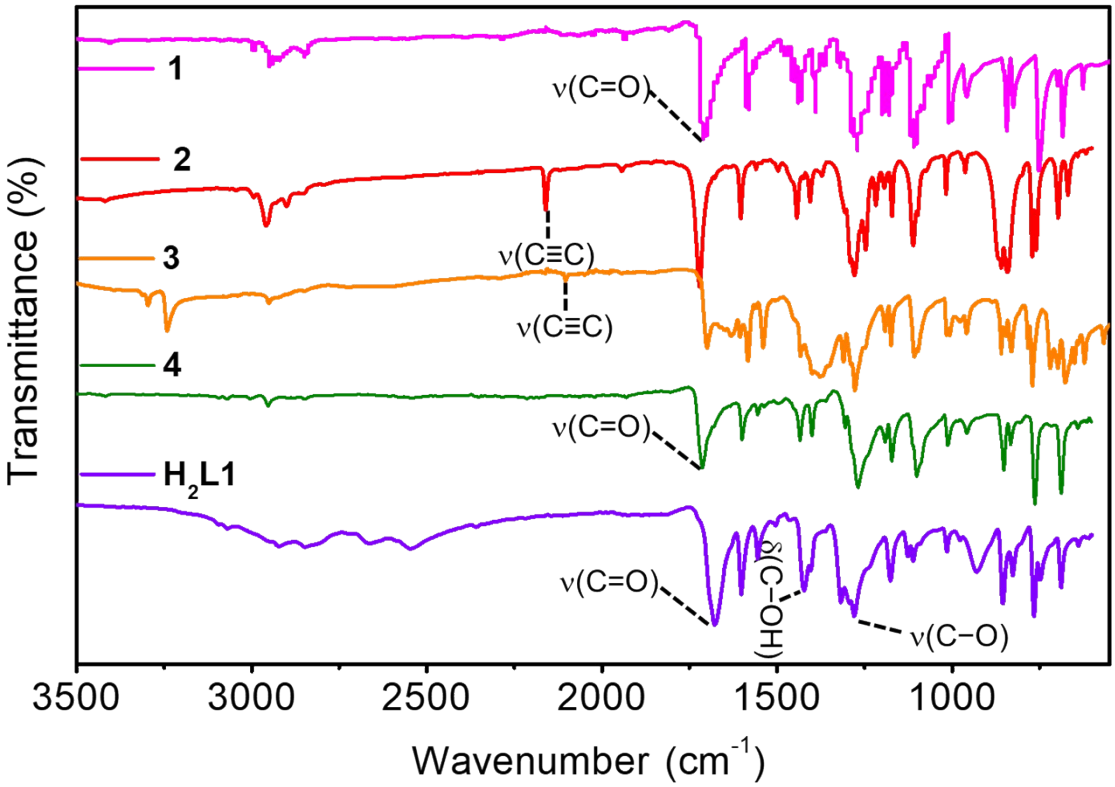

Fig. S1. ATR-FTIR spectra of the **H_2L1** proligand and its intermediates **1**, **2**, **3** and **4**.

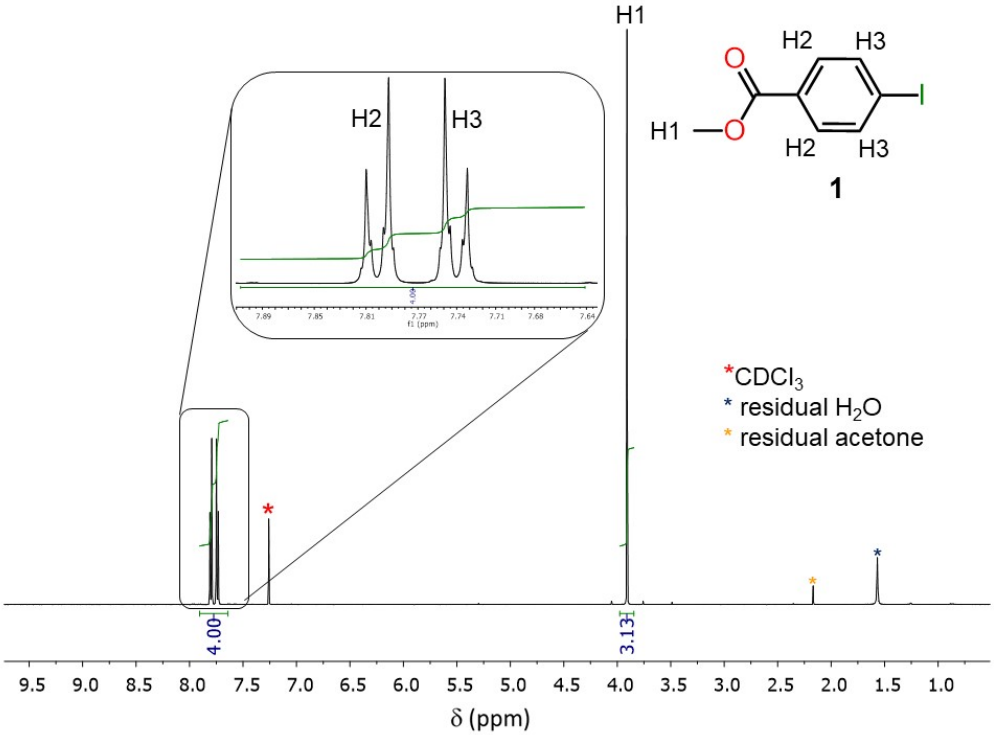

Fig. S2. ^{1}H NMR spectrum of the intermediate **1** in $CDCl_3$, at 298 K, in 500 MHz.

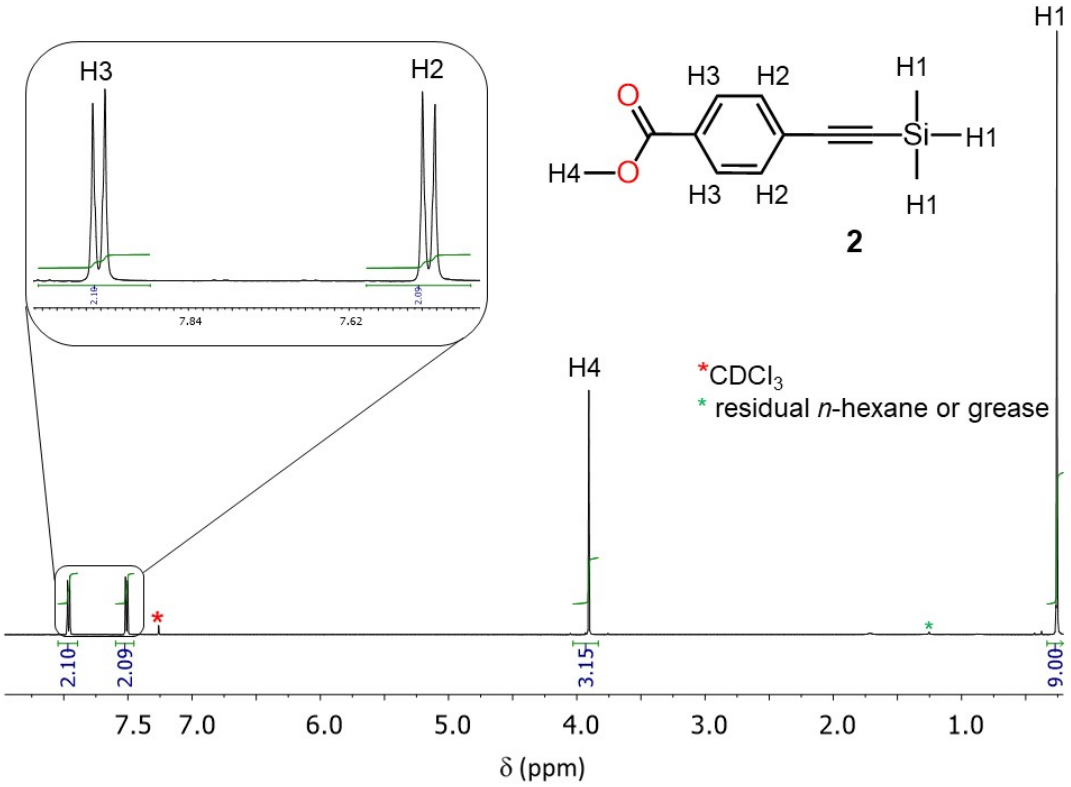

Fig. S3. ^{1}H NMR spectrum of the intermediate **2** in $CDCl_3$ at 298 K, in 500 MHz.

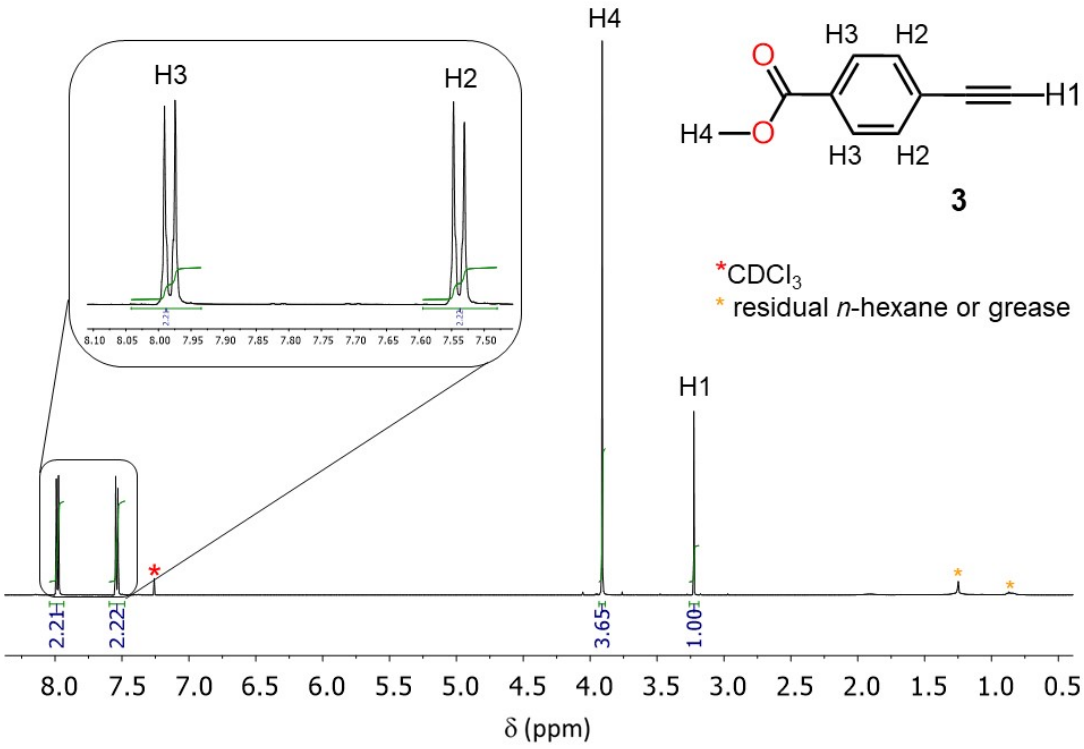

Fig. S4. ^{1}H NMR spectrum of the intermediate **3** in $CDCl_3$ at 298 K, in 500 MHz.

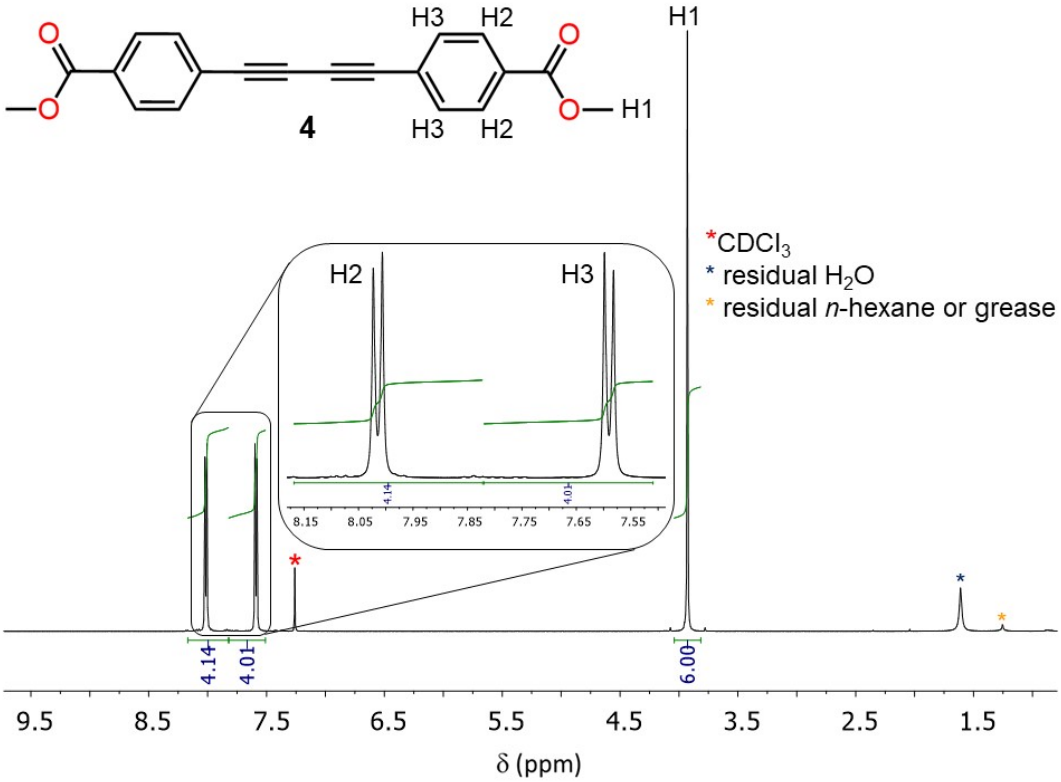

Fig. S5. ^{1}H NMR spectrum of the intermediate **4** in $CDCl_3$, at 298 K, in 500 MHz.

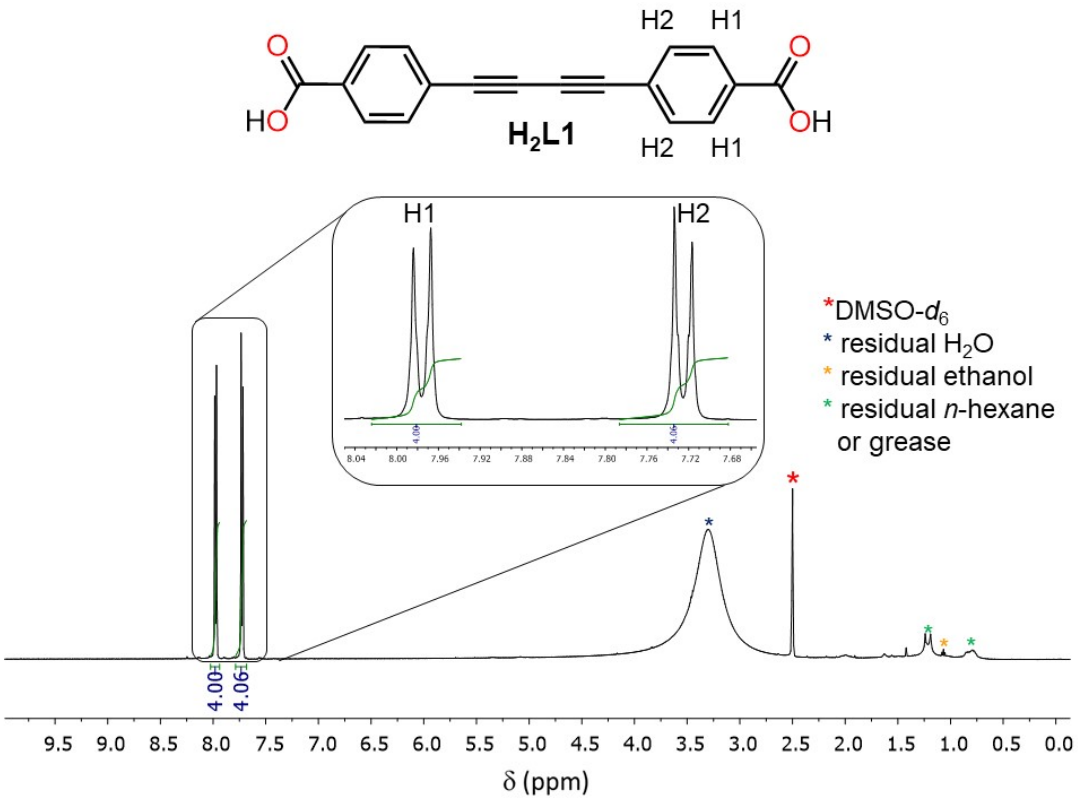

Fig. S6. ^{1}H NMR spectrum of the **H_2L1** proligand in DMSO-d_6 at 298 K, in 500 MHz.

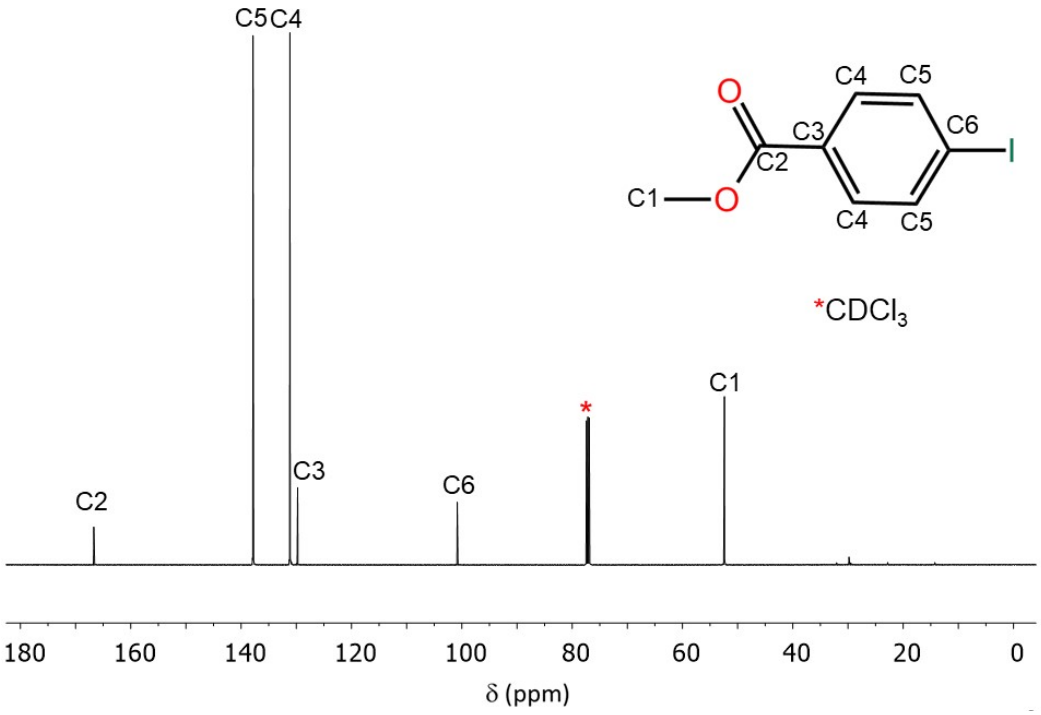

Fig. S7. ^{13}C NMR spectrum of the intermediate **1** in $CDCl_3$, at 298 K, in 125 MHz.

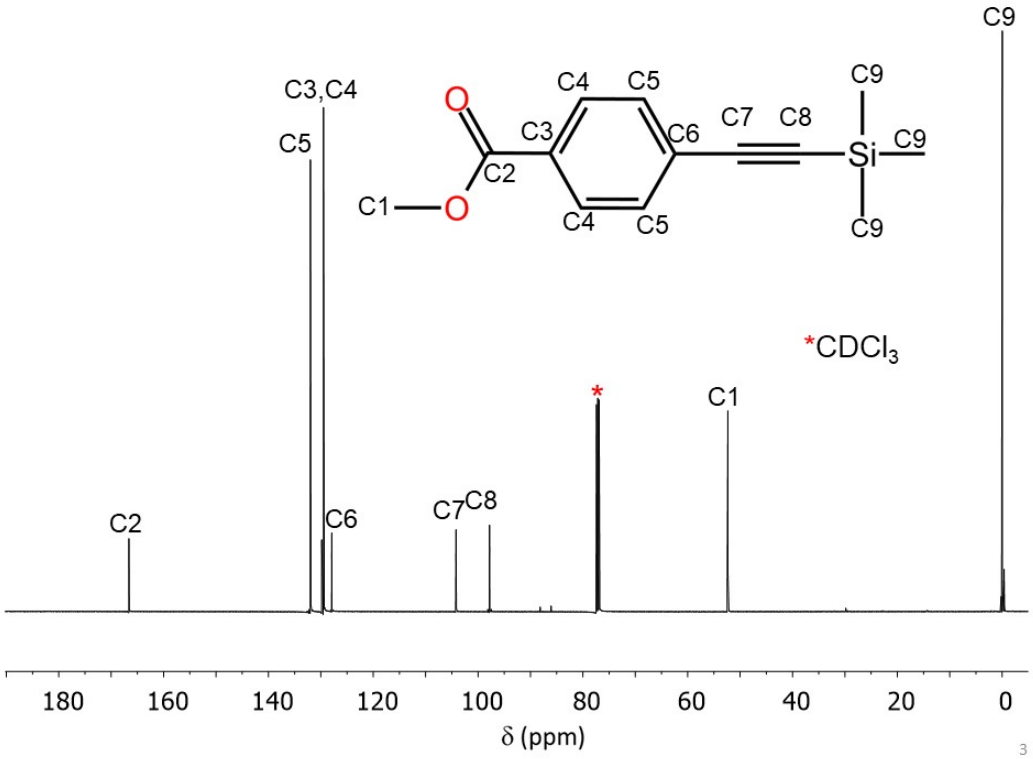

Fig. S8. ^{13}C NMR spectrum of the intermediate **2** in $CDCl_3$, at 298 K, in 125 MHz.

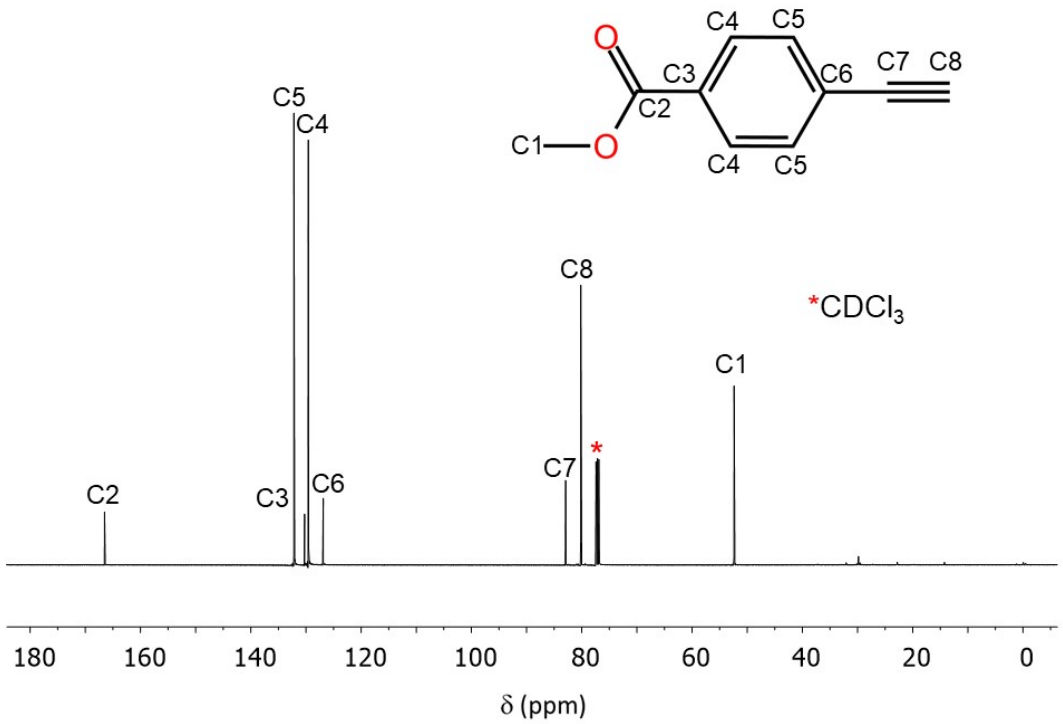

Fig. S9. ^{13}C NMR spectrum of the intermediate **3** in $CDCl_3$, at 298 K, in 125 MHz.

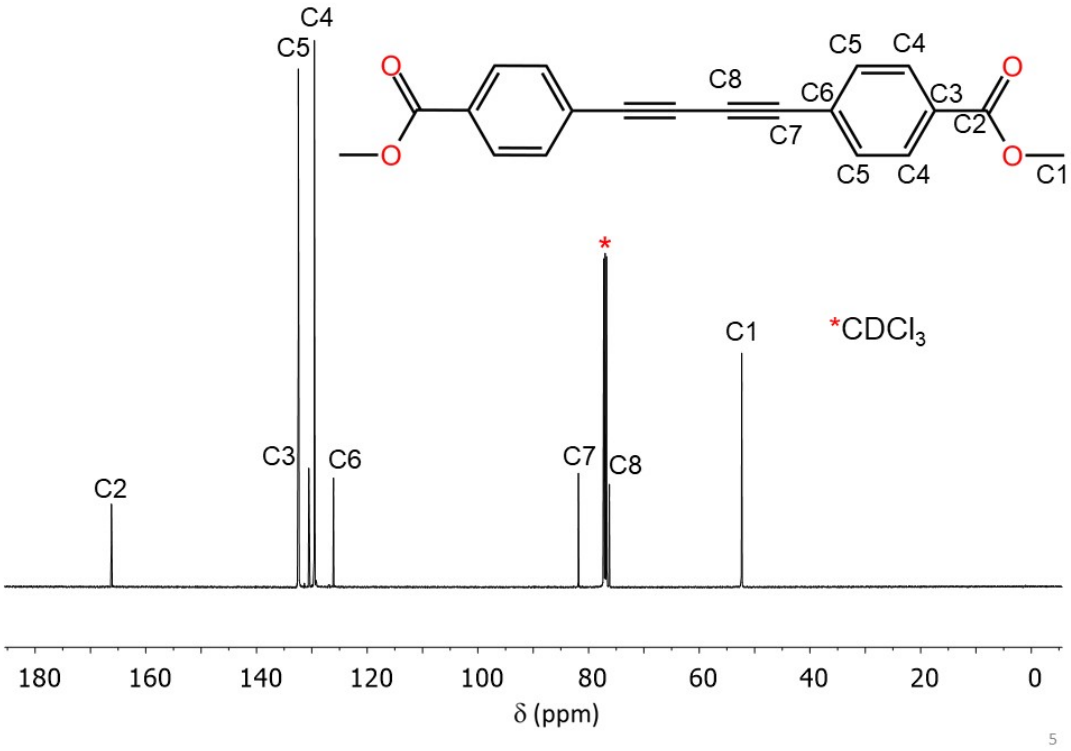

Fig. S10. ^{13}C NMR spectrum of the intermediate **4** in $CDCl_3$, at 298 K, in 125 MHz.

(a)

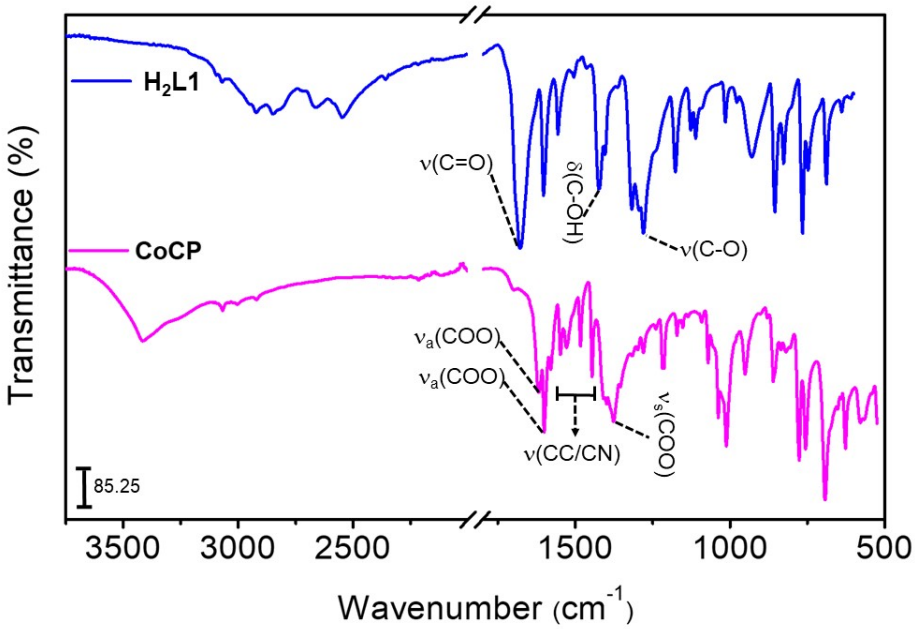

(b)

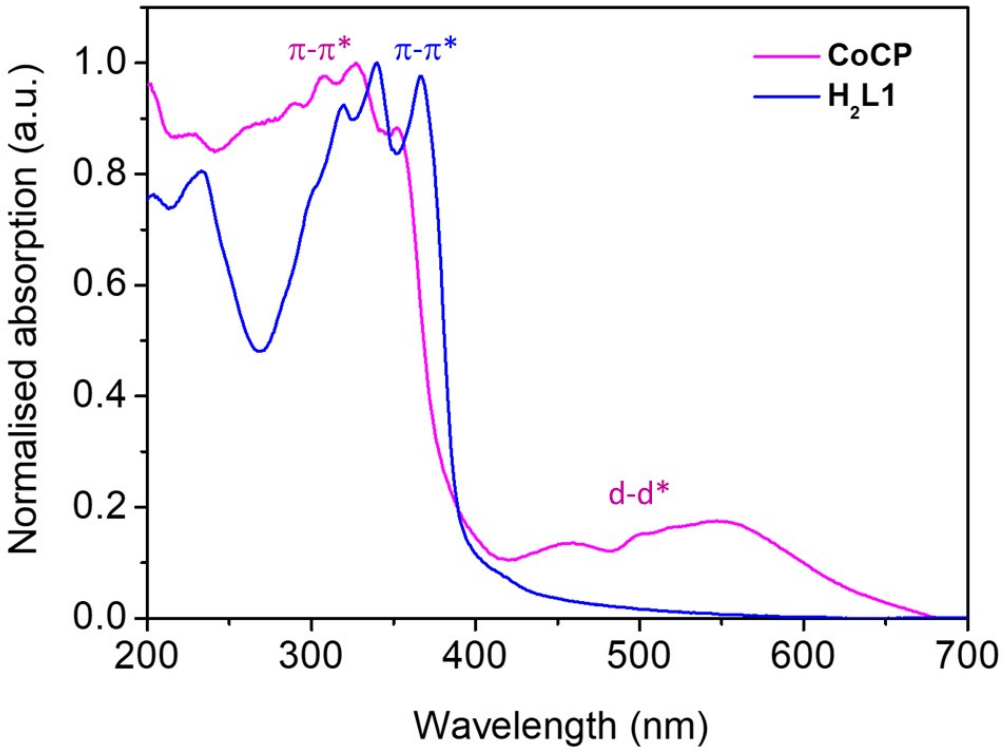

Fig. S11. (a) ATR-FTIR spectra with the main band assignments and (b) normalised UV−vis absorption spectra of the **H_2L1** proligand and the **CoCP**.

Table S1. Assignments of the main ATR-FTIR bands of the **H_2L1** and **CoCP**

H_2L1	**CoCP**	**Assignments**
1678	_	ν(C=O)
_	1618 and 1600	$\nu_a(COO^-)$
_	1579-1445	ν(CC/CN)
_	1398 and 1375	$\nu_s(COO^-)$
929	_	δ(O-H)

Table S2. Crystal data and structure refinement for the **CoCP** and intermediate **4**

Compounds	**4**	**CoCP**
Empirical formula	$C_{20}H_{14}O_4$	$C_{28}H_{20}CoN_2O_5$
Formula weight	318.31	523.39
Temperature/K	298(2)	298(2)
Crystal system	Triclinic	Monoclinic
Space group	$P\bar{1}$	$P2_1/n$
Unit cell dimensions	a = 7.0604(4) Å b = 10.6647(7) Å c = 11.8334(7) Å α = 75.773(3)° β = 73.159(2)° γ = 74.351(3)°	8.6551(3) Å 17.7754(5) Å 16.1528(5) Å α = 90° β=103.4240(10)° γ = 90°
Volume/Å^3	807.50(9)	2417.18(13)
Z	2	4
ρ calc./g cm^{-3}	1.3091	1.438
μ/mm^{-1}	0.091	0.752
F(000)	332.2	1076.0
Crystal size/mm^{-3}	0.280 x 0.254 x 0.164	0.313 x 0.167 x 0.162
Radiation	Mo Kα (λ = 0.71073)	Mo Kα (λ = 0.71073)
2Θ range for data collection/°	4.928 to 50.048°	4.584 to 50.046°
Reflections collected	23446	28501
Index ranges	-8 ≤ h ≤ 8, -12 ≤ k ≤ 12, -14 ≤ l ≤ 14	-10 ≤ h ≤ 10, -20 ≤ k ≤ 21, -19 ≤ l ≤ 19
Independent reflections	2853 [R_{int} = 0.0438, R_{sigma} = 0.0227]	4277 [R_{int} = 0.0334, R_{sigma} = 0.0198]
Data/restraints/parameters	2853/0/220	4277/1/328
Goof = S	1.112	1.036
Final R indexes [I ≥= 2σ (I)]	R_1 = 0.0553, wR_2 = 0.1416	R_1 = 0.0281, wR_2 = 0.0651
Final R indexes [all data]	R_1 = 0.0735, wR_2 = 0.1583	R_1 = 0.0343, wR_2 = 0.0688
Largest diff. peak/hole / e Å^{-3}	0.19/-0.20	0.34/-0.21

Table S3. Selected bond lengths (Å) in **CoCP**

Bond length			
Co1-OW	2.0877(14)	Co1-N2	2.1600(16)
Co1-O1	2.0239(12)	Co1-O3	2.1165(12)
Co1-N1	2.1348(15)	Co1-O4	2.3650(13)

Table S4. Bond Angles (°) in **CoCP**

Bond angles			
OW-Co1-O3	90.68(6)	N1-Co1-O4	148.82(5)
OW-Co1-O4	87.85(5)	N1-Co1-N2	94.39(6)
OW-Co1-N1	87.83(6)	N2-Co1-O4	91.72(5)
OW-Co1-N2	176.36(6)	C18-O3-Co1	95.93(11)
O3-Co1-O4	58.11(5)	C18-O4-Co1	84.90(11)
O3-Co1-N1	91.09(6)	C1-O1-Co1	130.18(13)
O3-Co1-N2	92.16(6)	C23-N1-Co1	119.57(13)
O1-Co1-OW	87.36(6)	C19-N1-Co1	122.07(14)
O1-Co1-O3	177.39(6)	C24-N2-Co1	120.65(14)
O1-Co1-O4	120.04(5)	C28-N2-Co1	123.01(14)
O1-Co1-N1	90.57(6)		
O1-Co1-N2	89.73(6)		

Crystal structure analyses of the intermediate 4. Suitable needle shaped single crystals of **4** were formed by slow evaporation in CH_2Cl_2 at room temperature. **4** crystallised in the $P\bar{1}$ with one molecule comprising the asymmetric unit (Fig. S12). The structure of **4** is non-planar as shown by the torsion angle between one phenyl ring and the adjacent

phenyl ring is 24.60°. The structure is stabilised by several supramolecular interactions including non-classical hydrogen bonds and π stacking such as: CH···O, CH···π and π···π listed in Fig. S12.

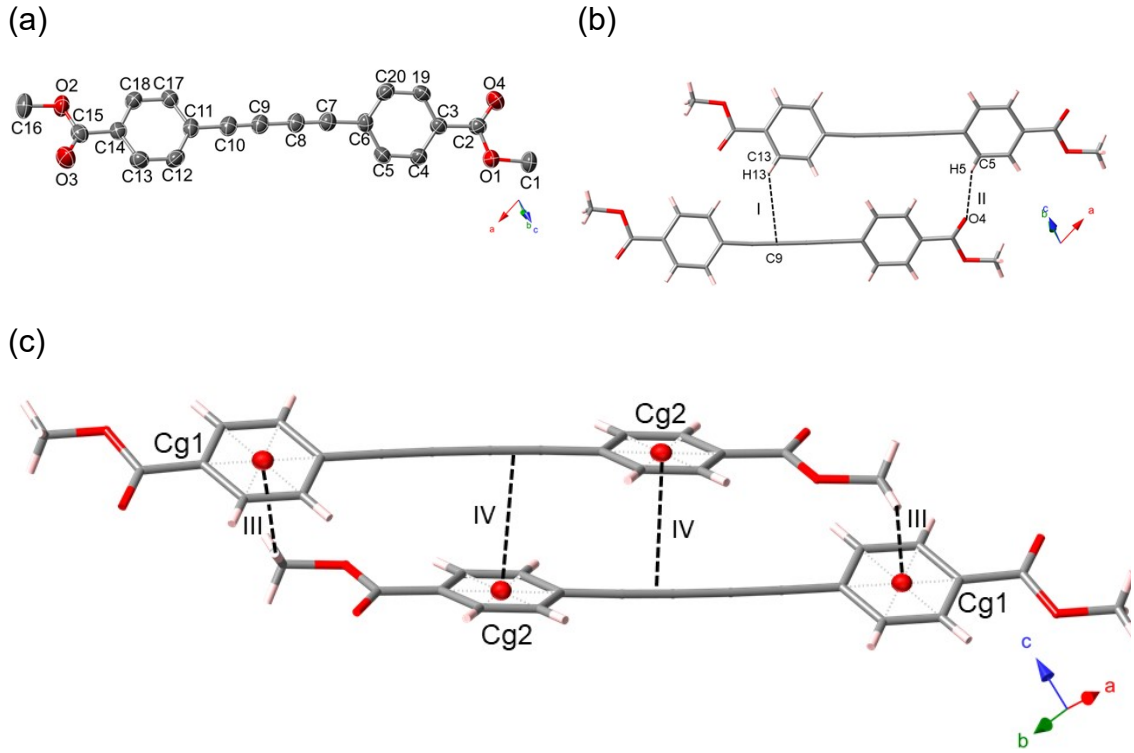

Fig. S12. (a) Asymmetric unit of **4**. Hydrogen atoms were hidden for the sake of clarity. Displacement ellipsoid parameters are drawn at the 50% probability level. Representation of hydrogen bonding (b) I (C13-H13···C9) and II (C5-H5···O4); (c) III (Cg···C1) and IV (Cg2···C8).

Fig. S12-b represents some non-classical hydrogen bonds type C-H···O and C-H···π named I (C13-H13···C9) and II (C5-H5···O4) with donor···acceptor distances of 3.940(4) Å and 3.194(4) Å, respectively. Fig. S12-c shows π···π stacking and C-H···π interactions named III (Cg1···C1) and IV (Cg2···C8) with distances 3.82(2) Å and 3.52(1) Å, respectively. These intermolecular interactions govern the crystal packing of the intermediate **4**.

Table S5. Selected bond lengths (Å) in **4**

Bond length			
O1-C1	1.445(3)	C7-C8	1.201(3)
O1-C2	1.328(3)	C8-C9	1.368(3)
O2-C15	1.333(3)	C9-C10	1.204(3)
O2-C16	1.439(3)	C10-C11	1.428(3)
O3-C15	1.197(3)	C11-C12	1.390(3)
O4-C2	1.193(3)	C11-C17	1.392(3)
C2-C3	1.486(3)	C12-C13	1.377(3)
C3-C4	1.381(3)	C13-C14	1.387(3)
C3-C19	1.390(3)	C14-C15	1.486(3)
C4-C5	1.377(3)	C14-C18	1.382(3)
C5-C6	1.396(3)	C17-C18	1.383(3)
C6-C7	1.429(3)	C19-C20	1.376(3)
C6-C20	1.386(3)		

Table S6. Selected bond angles (°) in **4**

Bond angles			
C2-O1-C1	116.73(19)	C9-C10-C11	178.8(3)
C15-O2-C16	115.9(2)	C12-C11-C10	121.0(2)
O1-C2-C3	112.41(19)	C12-C11-C17	119.1(2)
O4-C2-O1	122.7(2)	C17-C11-C10	119.9(2)
O4-C2-C3	124.9(2)	C13-C12-C11	120.4(2)
C4-C3-C2	122.2(2)	C12-C13-C14	120.4(2)
C4-C3-C19	119.3(2)	C13-C14-C15	118.2(2)
C19-C3-C2	118.44(19)	C18-C14-C13	119.4(2)
C5-C4-C3	120.3(2)	C18-C14-C15	122.3(2)
C4-C5-C6	120.5(2)	O2-C15-C14	112.7(2)
C5-C6-C7	119.5(2)	O3-C15-O2	123.0(2)
C20-C6-C5	118.9(2)	O3-C15-C14	124.3(2)
C20-C6-C7	121.7(2)	C18-C17-C11	120.1(2)
C8-C7-C6	176.5(3)	C14-C18-C17	120.5(2)
C7-C8-C9	178.9(3)	C20-C19-C3	120.5(2)
C10-C9-C8	178.7(3)	C19-C20-C6	120.5(2)

(a)

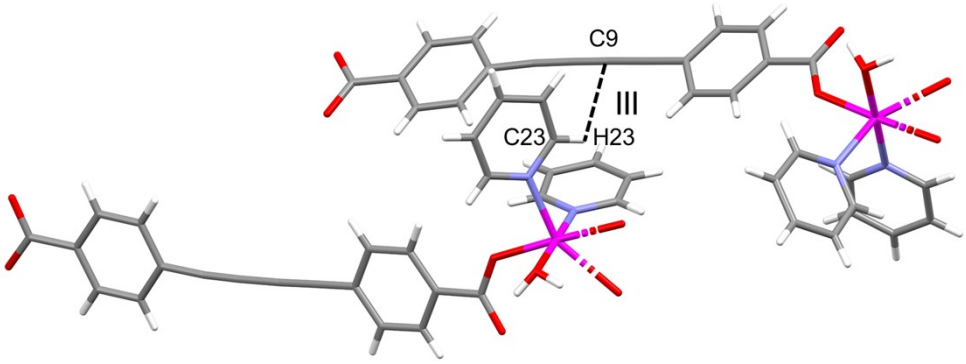

(b)

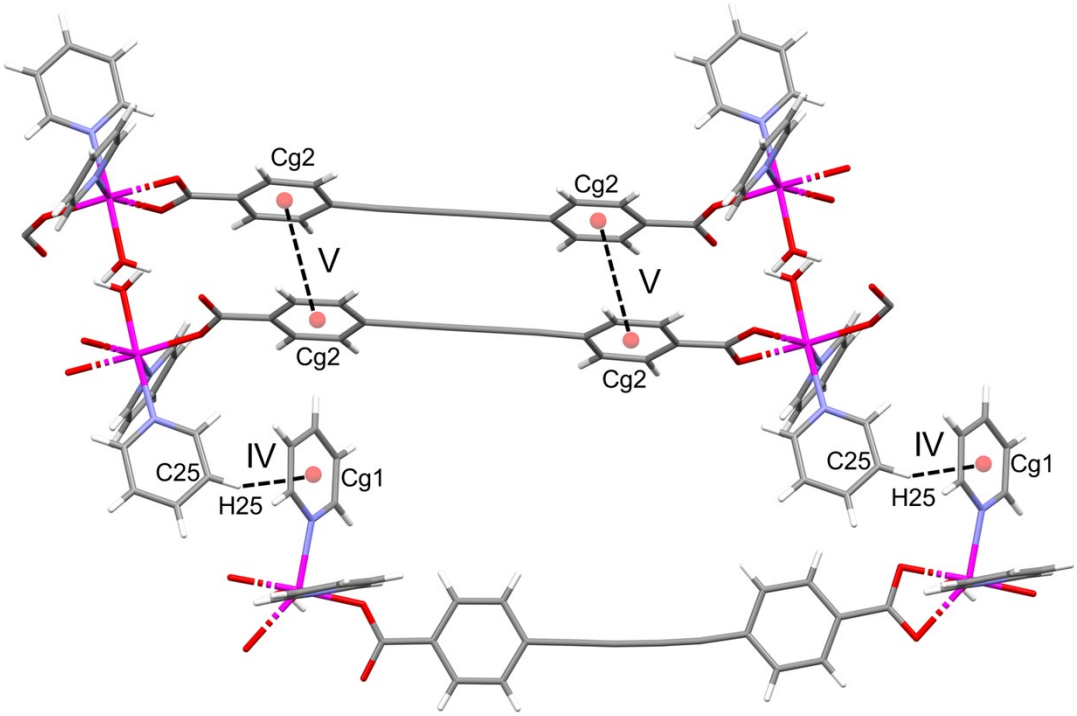

Fig. S13. Representation of the interactions (a) III, (b) IV and V in compound **CoCP**.

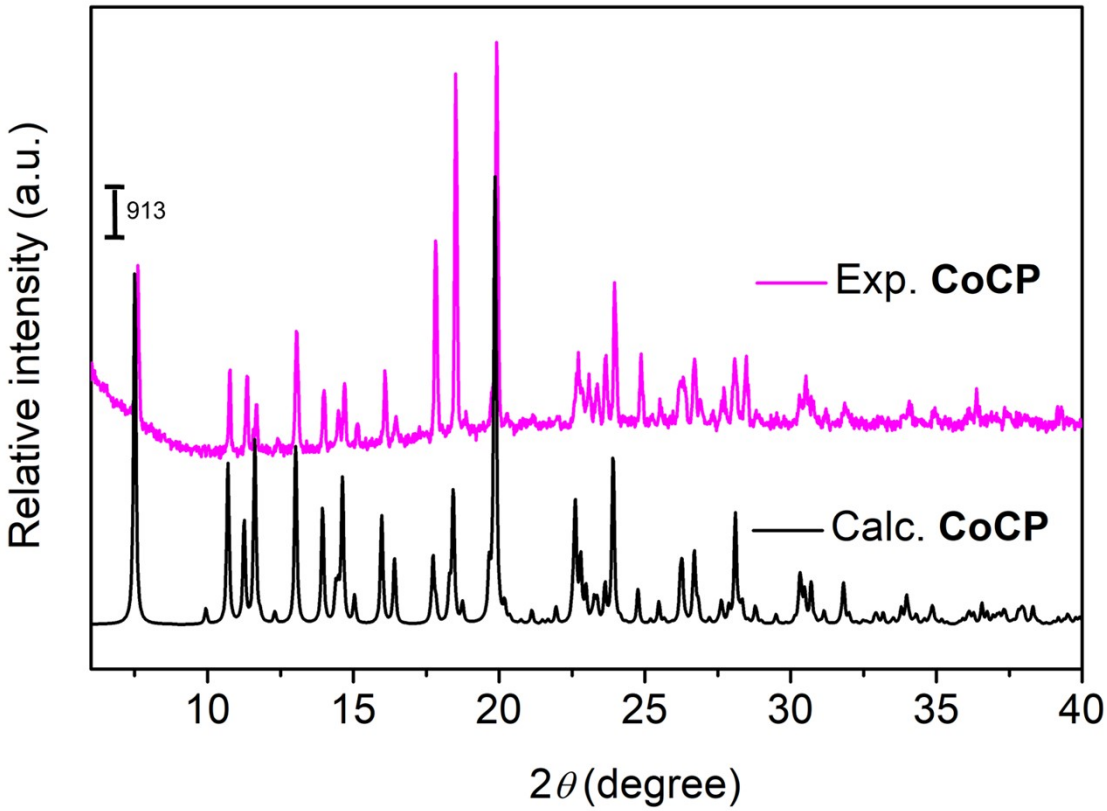

Fig. S14. Calculated PXRD generated from single crystal structure of the **CoCP (**Calc. **CoCP)** compared with experimental data (Exp. **CoCP**).

Table S7. Hydrogen bonds and short contacts in **CoCP** (distances are given in Å and angles in °).

Interaction	d (D···H/A)	d (D-H)[a]	d (H···A)[b]	d (D···A)[c]
I	OW-HWA···O4	0.80(3)	2.02(3)	2.774(2)
II	OW-HWB···O2	0.80(3)	1.83(3)	2.629(2)
III	C23-H23···C9	-	-	3.430(3)
IV	C25-H25···Cg1	-	-	3.57(1)
V	Cg2···Cg2	-	-	3.78(2)

[a] Distance between the donor atom and the hydrogen atom.
[b] Distance between the acceptor atom and the hydrogen atom.
[c] Distance between the donor atom and the acceptor atom for **I**, **II** and **III** or the distance between the donor atom and the centroid (Cg) for **IV** and **V**.

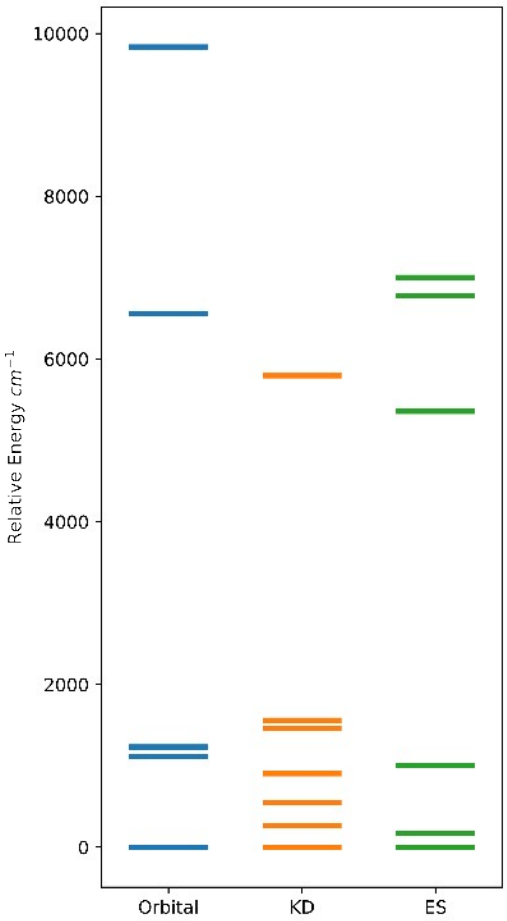

Fig. S15. Relative energies obtained for the **CoCP** compound: (blue) 3d orbitals; (orange) Kramers doublets; (green) transition energies. All energies are relative to the ground (0.0 cm^{-1}) energy.

Table S8. Energy gap between the first 7 excited states and the ground state of compound **CoCP**

STATE	ROOT	MULT	DE/eV	DE/cm^{-1}
1	1	4	0.024	195.5
2	2	4	0.16	1290.6
3	3	4	0.863	6958.9
4	4	4	1.082	8729
5	5	4	1.11	8953
6	0	2	1.228	9903.6
7	1	2	1.635	13189.5

Table S9. First 12 eigenvalues of the Kramers doublets

Eigenvalues	cm^{-1}	eV
0	0	0
1	0	0
2	246.54	0.0306
3	246.54	0.0306
4	555.32	0.0689
5	555.32	0.0689
6	866.9	0.1075
7	866.9	0.1075
8	1700.25	0.2108
9	1700.25	0.2108
10	1777.96	0.2204
11	1777.96	0.2204
12	7344.9	0.9107

Table S10. Description of the ground Kramers doublet

	Eigenvector				
	Weight	**Block**	**Root**	**Spin**	**Ms**
KD 0	0.559	0	0	3/2	3/2
	0.360	0	1	3/2	3/2
	0.035	0	2	3/2	1/2
	0.020	0	0	3/2	-1/2
	0.013	0	1	3/2	-1/2

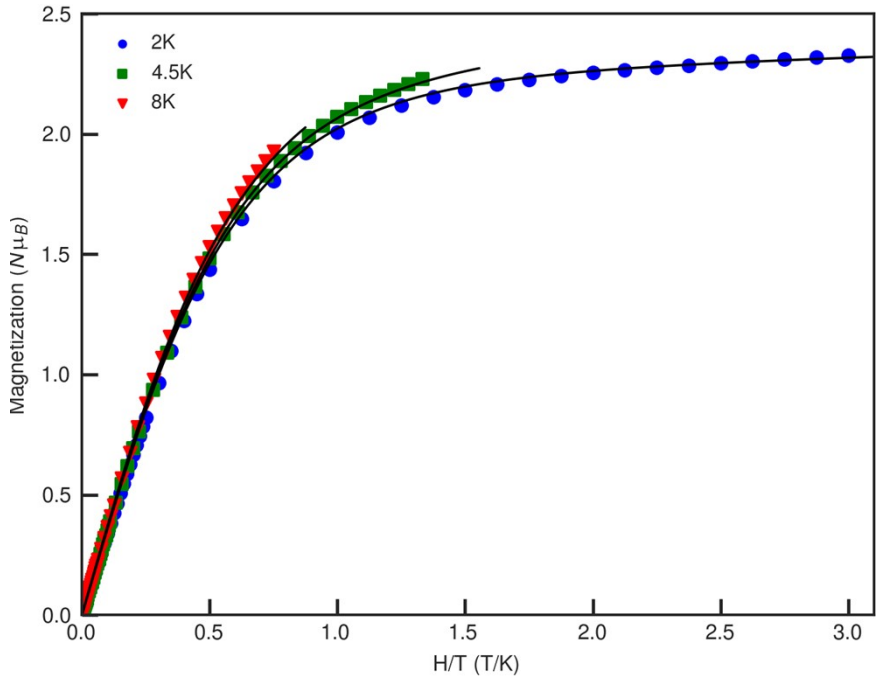

Fig. S16. Magnetization results obtained for **CoCP**.The lines represent the fitted values obtained with PHI.

Table S11. Selected magnetic results of hexacoordinated octahedral complexes with easy-axis anisotropy.

Compound	σ	λ / cm^{-1}	Δ_{ax}/cm^{-1}	Δ_{rh}/cm^{-1}	zJ/cm^{-1}	Ab Initio	Ref
CoCP	−1.5	−146.8(4)	−1054(5)	-151.4(5)		Yes	This work
cis-[Co(hfac)$_2$(H$_2$O)$_2$]	1.34	-147.2	-499.7	136.3		Yes	[1]
[Co(dca)$_2$(bim)$_4$]	-1.18	-132.0	-416.3			No	[2]
[Co(dca)$_2$(bim)$_2$]$_n$	-1.16	-134.1	-402.7			No	[2]
[Co(dca)$_2$(bmim)$_2$]$_n$	-1.24	-134.0	-605.8			No	[2]
[Co(dca)$_2$(atz)$_2$]$_n$	-1.18(1)	-125(1)	-509(10)			No	[3]
[Co(ppad)$_2$]$_n$	-1.48(1)	-147(1)	-428(5)			No	[4]
[Co(AcO)$_2$(py)$_2$(H$_2$O)$_2$]	-1.5	-170	-279	109		Yes	[5]
[Co(pydm)$_2$](dnbz)$_2$	-0.61	-187	-585			Yes	[6]
(NBu$_4$)[Co(piv)$_3$]	1.33	-170	-713.2	66.3		Yes	[7]

Abbreviations: hfac = hexafluoroacetylacetonate; dca = dicyanamide; bim = 1-benzylimidazole; bmim = 1-benzyl-2-methylimidazole; atz = 2-amino-1,3,5-triazine; ppad = N3-(3-pyridoyl)-3-pyridinecarboxamidrazone; AcO = acetate anion; py = pyridyl; pydm = 2,6-pyridinedimethanol; dnbz = 3,5-dinitrobenzoato(1-); ac = acetato; Melm = 1-methylimidazole; piv = pivalato

Table S12. Percentage composition of the eigenstates for **CoCP.**

E/cm^{-1}		0.0	0.0	185.3	185.3	533.4	533.4	785.8	785.8	1551	1551	1607	1607
m_S	m_L												
-1.5	-1.0	3.39	0.00	0.59	0.00	0.00	0.17	95.75	-	0.00	0.00	0.09	-
-1.5	0.0	-	0.02	0.00	0.80	5.89	0.12	-	0.01	0.42	90.42	-	2.32
-1.5	1.0	84.44	0.00	8.45	0.00	0.01	0.36	3.72	-	0.10	0.00	2.92	-
-0.5	-1.0	0.00	0.64	0.01	18.46	72.59	1.43	-	0.03	0.03	6.30	-	0.51
-0.5	0.0	4.91	0.00	1.97	0.00	0.03	1.46	0.31	-	2.70	0.01	88.61	-
-0.5	1.0	0.00	6.60	0.03	69.70	17.59	0.35	-	0.18	0.00	0.01	-	5.54
0.5	-1.0	6.60	0.00	69.70	0.03	0.35	17.59	0.18	-	0.01	0.00	5.54	-
0.5	0.0	0.00	4.91	0.00	1.97	1.46	0.03	-	0.31	0.01	2.70	-	88.61
0.5	1.0	0.64	0.00	18.46	0.01	1.43	72.59	0.03	-	6.30	0.03	0.51	-
1.5	-1.0	0.00	84.44	0.00	8.45	0.36	0.01	-	3.72	0.00	0.10	-	2.92
1.5	0.0	0.02	-	0.80	0.00	0.12	5.89	0.01	-	90.42	0.42	2.32	-
1.5	1.0	0.00	3.39	0.00	0.59	0.17	0.00	-	95.75	0.00	0.00	-	0.09

Table S13. G-tensors of the Kramer doublets for **CoCP**.

E/cm^{-1}	g_X	g_Y	g_Z
0.0	1.9	2.5	7.5
185.3	1.7	2.5	4.4
533.4	0.4	3.1	3.9
785.8	0.2	0.2	3.2
1551	0.7	0.9	5.3
1607	1.6	2.1	3.6

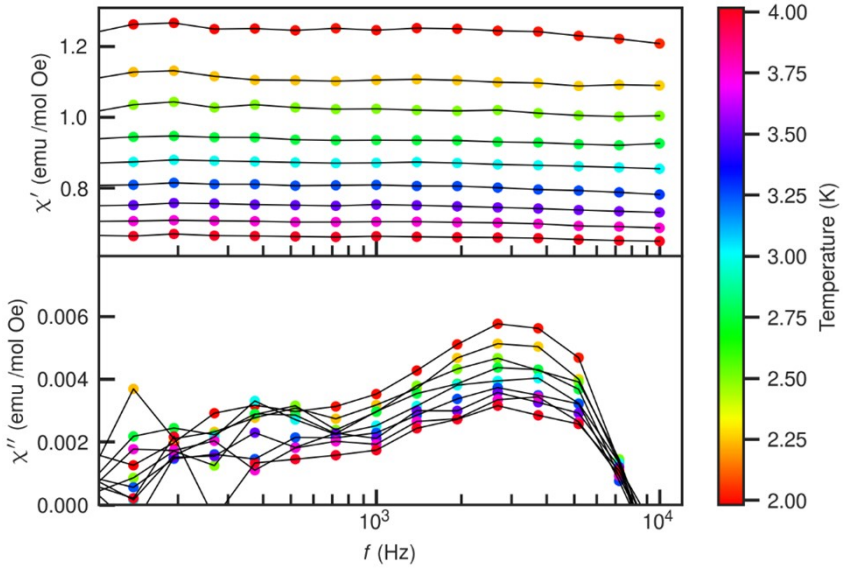

Fig. S17. Frequency-dependence of AC susceptibility for **CoCP** measured at zero DC field (lines are guides for the eyes).

Table S14. Cole-Cole parameters obtained from fits of the frequency-dependence of χ_{AC} (measured at 450 Oe) using a Generalized Debye model and used to reproduce the Cole-Cole plots.

Temperature (K)	χ_S (emu/K Oe)	χ_T (emu/K Oe)	α	τ(s)
2.75	0.52	0.65	0.12	2.81×10^{-4}
3.00	0.48	0.60	0.10	2.40×10^{-4}
3.25	0.44	0.56	0.11	1.88×10^{-4}
3.50	0.41	0.52	0.11	1.56×10^{-4}
3.75	0.39	0.49	0.08	1.27×10^{-4}
4.00	0.36	0.46	0.08	1.04×10^{-4}
4.25	0.34	0.44	0.07	8.41×10^{-5}
4.50	0.33	0.42	0.06	6.73×10^{-5}
4.75	0.31	0.39	0.06	5.35×10^{-5}
5.00	0.30	0.38	0.05	4.32×10^{-5}
5.50	0.27	0.34	0.04	2.70×10^{-5}

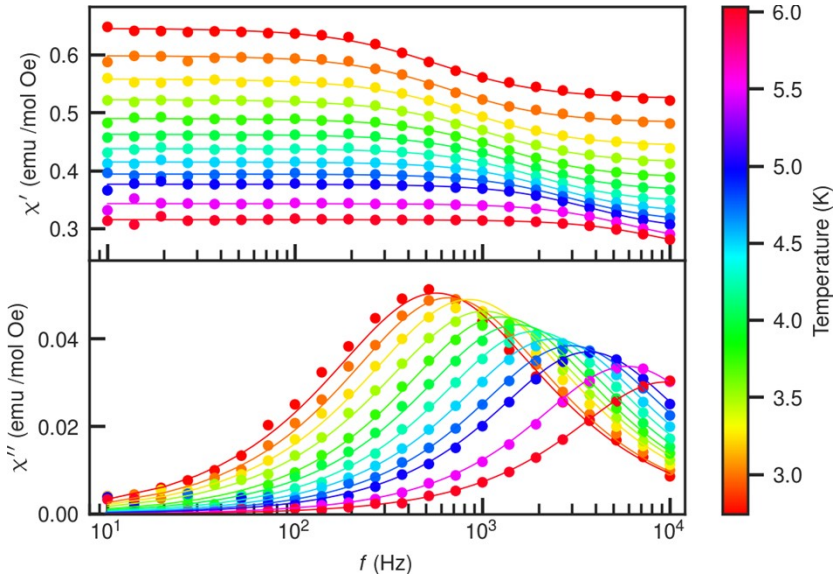

Fig. S18. Frequency-dependence of AC susceptibility for **CoCP** measured at 450 Oe (lines represent the fits made using a generalized Debye model).

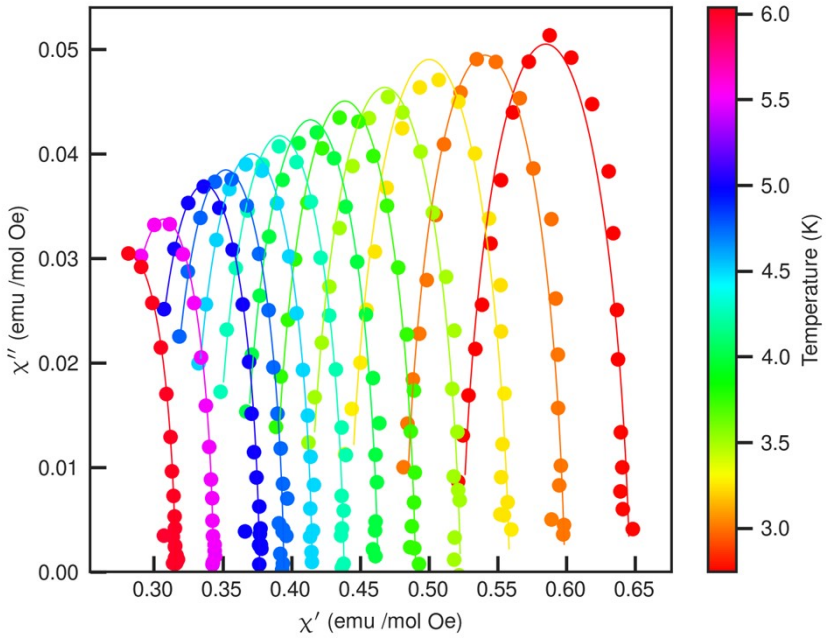

Fig. S19. Cole-Cole plot obtained from the frequency-dependence of χ_{AC} susceptibility for **CoCP** measured at 450 Oe (lines represent the fits made using a generalized Debye model).

Table S15. Cole-Cole parameters obtained from fits of the frequency-dependence of χ_{AC} (measured at 1kOe) using a Generalized Debye model.

Temperature (K)	χ_S (emu/K Oe)	χ_T (emu/K Oe)	α	τ(s)
2.25	0.55	0.99	0.15	4.25×10^{-4}
2.50	0.50	0.94	0.13	3.83×10^{-4}
2.75	0.46	0.90	0.12	3.28×10^{-4}
3.00	0.41	0.85	0.11	2.70×10^{-4}
3.25	0.38	0.80	0.11	2.21×10^{-4}
3.50	0.36	0.76	0.10	1.87×10^{-4}
3.75	0.33	0.72	0.10	1.52×10^{-4}
4.00	0.31	0.68	0.09	1.22×10^{-4}
4.25	0.30	0.64	0.08	9.82×10^{-5}
4.50	0.28	0.61	0.08	7.82×10^{-5}
4.75	0.27	0.58	0.06	6.17×10^{-5}
5.00	0.25	0.55	0.06	4.82×10^{-5}
5.50	0.23	0.50	0.05	2.91×10^{-5}
6.00	0.21	0.46	0.04	1.79×10^{-5}

Table S16. Cole-Cole parameters obtained from fits of the frequency-dependence of χ_{AC} (measured at 2kOe) using a Generalized Debye model and used to reproduce the Cole-Cole plots.

T (K)	$\chi_{S,T}$ (emu/K)	$\Delta\chi_{T1}$ (emu/K)	τ_1 (s)	α_1	$\Delta\chi_{T2}$ (emu/K)	τ_2 (s)	α_2
2.0	0.196	0.285	3.08×10^{-4}	0.175	0.822	0.40	0.54
2.2	0.179	0.313	2.96×10^{-4}	0.152	0.556	0.21	0.55
2.4	0.164	0.352	2.86×10^{-4}	0.149	0.730	1.15	0.57
2.6	0.153	0.386	2.68×10^{-4}	0.149	0.707	1.65	0.51
2.8	0.142	0.398	2.45×10^{-4}	0.141	0.559	3.11	0.55
3.0	0.133	0.413	2.23×10^{-4}	0.146	0.816	4.24	0.37
3.2	0.125	0.411	1.98×10^{-4}	0.140	-	-	-
3.4	0.118	0.406	1.74×10^{-4}	0.137	-	-	-
3.6	0.112	0.396	1.51×10^{-4}	0.132	-	-	-
3.8	0.107	0.383	1.30×10^{-4}	0.124	-	-	-
4.0	0.103	0.368	1.12×10^{-4}	0.112	-	-	-
4.5	0.095	0.335	0.74×10^{-4}	0.091	-	-	-
5	0.089	0.304	0.48×10^{-4}	0.065	-	-	-
5.5	0.083	0.279	0.30×10^{-4}	0.049	-	-	-
6	0.078	0.256	0.19×10^{-4}	0.0372	-	-	-

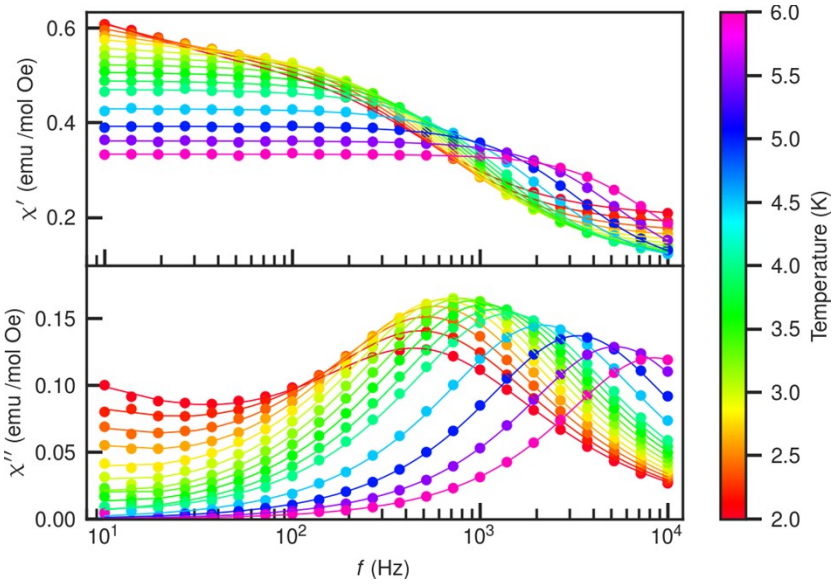

Fig. S20. Frequency-dependence of AC susceptibility for **CoCP** measured at 2 kOe (lines represent the fits made using a generalized Debye model).

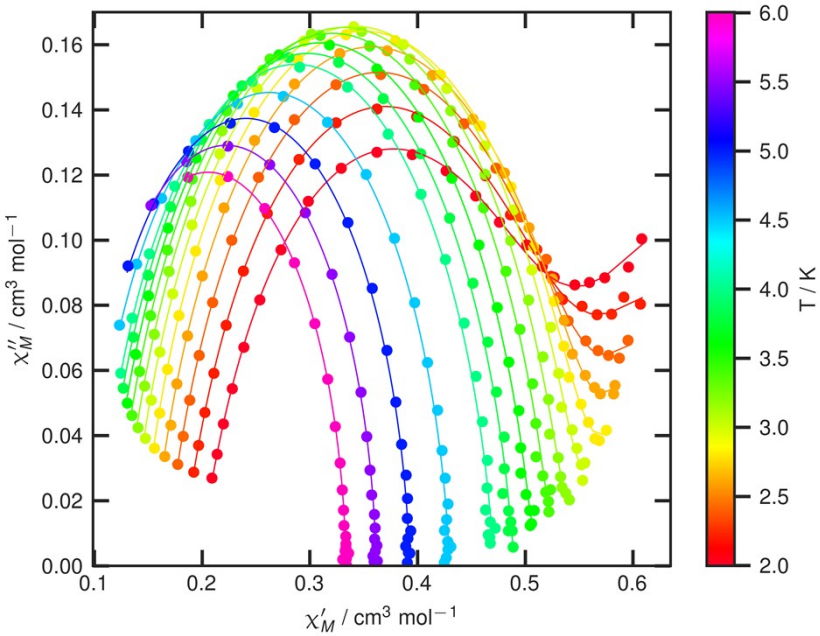

Fig. S21. Cole-Cole plot obtained from the frequency-dependence of χ_{AC} susceptibility for **CoCP** (measured at 2 kOe) (lines represent the fits made using a generalized Debye model).

Table S17. Cole-Cole parameters obtained from fits of the frequency-dependence of χ_{AC} (measured at 3 kOe) using a Generalized Debye model.

T (K)	$\chi_{S,T}$ (emu/K)	$\Delta\chi_{T1}$ (emu/K)	τ_1 (s)	α_1	$\Delta\chi_{T2}$ (emu/K)	τ_2 (s)	α_2
2.0	0.092	0.242	1.65×10^{-4}	0.238	0.39	0.05	0.33
2.2	0.083	0.237	1.63×10^{-4}	0.173	4.34	57.9	0.60
2.4	0.075	0.267	1.69×10^{-4}	0.151	3.59	88.3	0.63
2.6	0.072	0.319	1.76×10^{-4}	0.158	5.39	162.8	0.57
2.8	0.068	0.350	1.73×10^{-4}	0.151	5.61	200.3	0.55
3.0	0.065	0.376	1.67×10^{-4}	0.148	6.06	260.1	0.52
3.2	0.061	0.394	1.57×10^{-4}	0.147	-	-	-
3.4	0.058	0.402	1.44×10^{-4}	0.144	-	-	-
3.6	0.055	0.405	1.31×10^{-4}	0.140	-	-	-
3.8	0.052	0.400	1.16×10^{-4}	0.135	-	-	-
4.0	0.051	0.391	1.02×10^{-4}	0.125	-	-	-
4.5	0.048	0.364	0.70×10^{-4}	0.102	-	-	-
5	0.047	0.335	0.46×10^{-4}	0.077	-	-	-
5.5	0.045	0.309	0.30×10^{-4}	0.056	-	-	-
6	0.042	0.285	0.19×10^{-4}	0.044	-	-	-

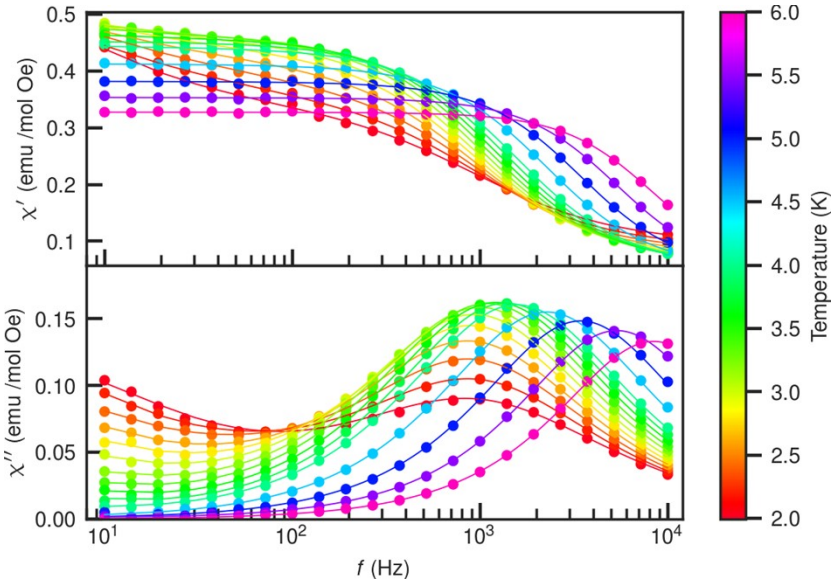

Fig. S22. Frequency-dependence of AC susceptibility for **CoCP** measured at 3 kOe (lines represent the fits made using a generalized Debye model).

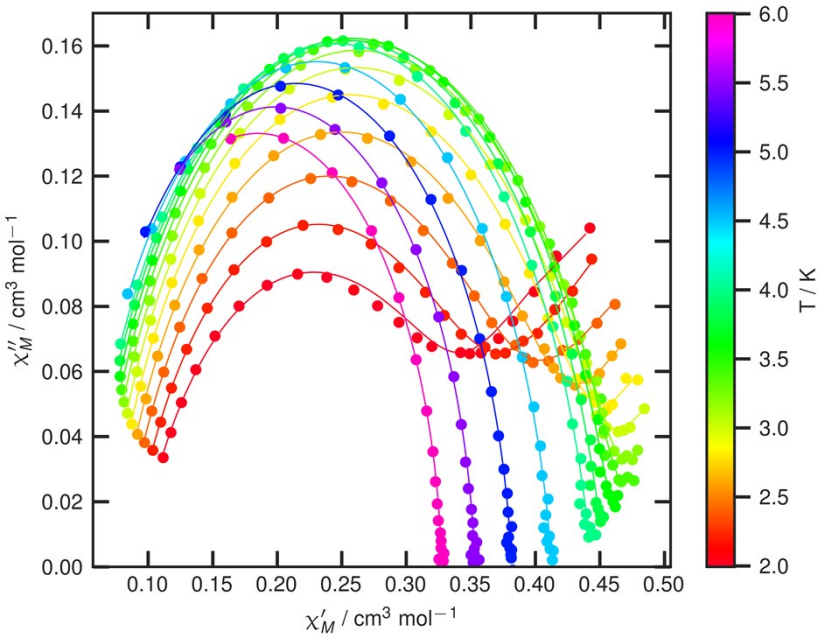

Fig. S23. Cole-Cole plot obtained from the frequency-dependence of χ_{AC} susceptibility for **CoCP** (measured at 3 kOe) (lines represent the fits made by using a generalized Debye model).

Table S18. Cole-Cole parameters obtained from fits of the frequency-dependence of χ_{AC} (measured at 2.7 K) using a Generalized Debye model.

H (Oe)	$\chi_{S,T}$ (emu/K)	$\Delta\chi_{T1}$ (emu/K)	τ_1 (s)	α_1	$\Delta\chi_{T2}$ (emu/K)	τ_2 (s)	α_2
350	0.61	0.09	2.83×10^{-4}	0.18	-	-	-
450	0.52	0.65	2.81×10^{-4}	0.12	-	-	-
550	0.52	0.17	3.09×10^{-4}	0.12	-	-	-
750	0.44	0.24	3.24×10^{-4}	0.12	-	-	-
1000	0.31	0.62	3.28×10^{-4}	0.12	-	-	-
1100	0.31	0.34	3.27×10^{-4}	0.13	-	-	-
1200	0.29	0.36	3.26×10^{-4}	0.13	-	-	-
1300	0.26	0.37	3.23×10^{-4}	0.13	-	-	-
1400	0.24	0.39	3.20×10^{-4}	0.14	-	-	-
1500	0.22	0.40	3.16×10^{-4}	0.14	-	-	-
1600	0.20	0.40	3.01×10^{-4}	0.13	0.13	0.13	0.25
1700	0.18	0.40	2.93×10^{-4}	0.13	9.35	49.46	0.27
1800	0.17	0.39	2.85×10^{-4}	0.13	2.88	126.34	0.51
1900	0.16	0.40	2.80×10^{-4}	0.13	5.99	48.16	0.34
2000	0.14	0.40	2.69×10^{-4}	0.13	5.66	65.38	0.39
2200	0.12	0.40	2.54×10^{-4}	0.14	8.48	55.25	0.33
2400	0.11	0.39	2.38×10^{-4}	0.14	6.52	69.55	0.39
2600	0.09	0.37	2.17×10^{-4}	0.14	8.09	100.90	0.42
2800	0.08	0.36	2.00×10^{-4}	0.15	9.31	135.11	0.42
3000	0.07	0.35	1.82×10^{-4}	0.14	11.02	166.10	0.43
3200	0.06	0.34	1.67×10^{-4}	0.15	16.24	155.81	0.38
3400	0.05	0.32	1.49×10^{-4}	0.14	20.75	597.11	0.45
3600	0.05	0.31	1.35×10^{-4}	0.15	20.61	211.87	0.39
3800	0.04	0.29	1.21×10^{-4}	0.14	14.09	341.10	0.46
4000	0.04	0.28	1.11×10^{-4}	0.14	18.20	321.97	0.43
4200	0.03	0.27	1.01×10^{-4}	0.14	24.92	311.93	0.39
4400	0.03	0.25	9.09×10^{-5}	0.12	12.05	516.65	0.50
4600	0.03	0.24	8.28×10^{-5}	0.13	16.75	347.63	0.44
4800	0.03	0.22	7.50×10^{-5}	0.12	16.02	608.18	0.48
5000	0.02	0.22	6.83×10^{-5}	0.13	24.92	671.52	0.43

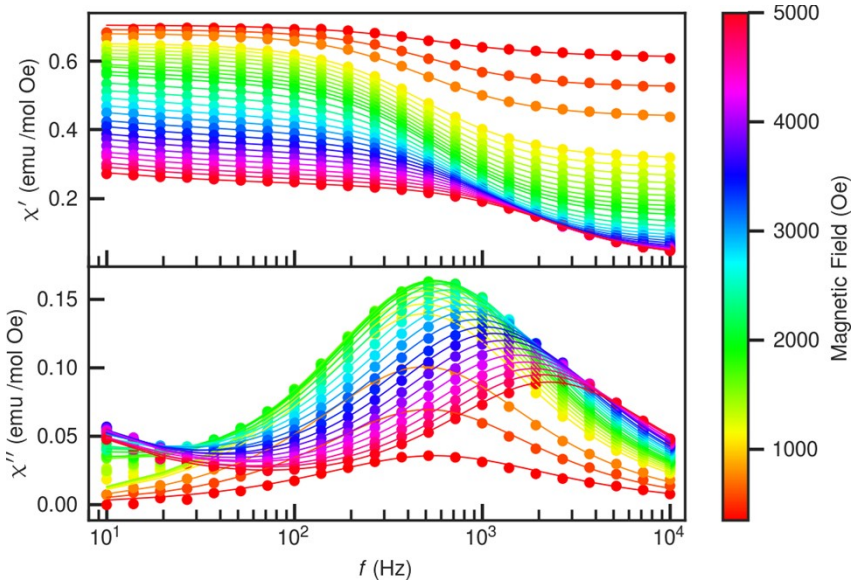

Fig. S24. Frequency-dependence of AC susceptibility for **CoCP** measured at 2.7 K (lines represent the fits made using a generalized Debye model).

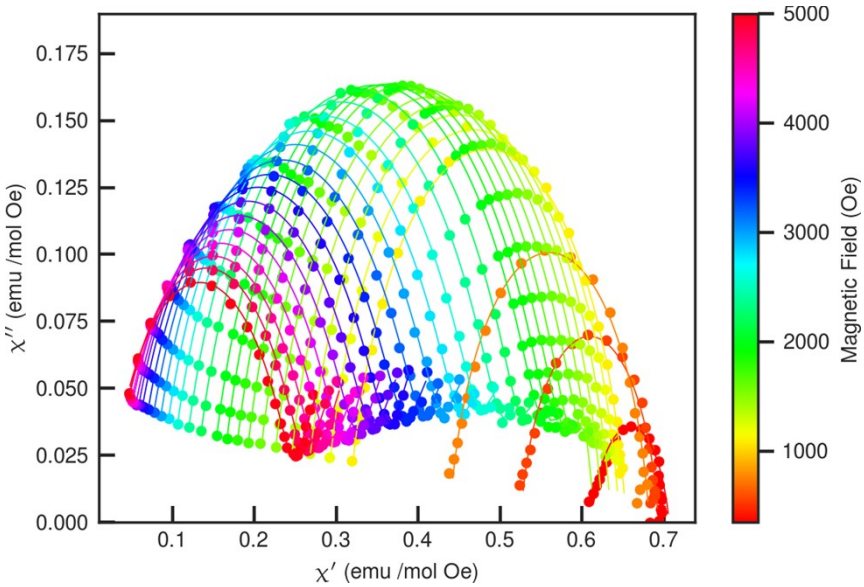

Fig. S25. Cole-Cole plot obtained from the frequency-dependence of χ_{AC} susceptibility for **CoCP** (measured at 2.7 K) (lines represent the fits made using a generalized Debye model).

Table S19. Selected magnetic data of dynamic magnetic properties and structural correlations of hexacoordinated octahedral complexes.

Compound	τ_0/ s	B_{DC}/T	U_{ff}/ cm^{-1}	*A*/ s^{-1} K^{-1}	*C* / s^{-1} K^{-n}	*n*	τ_{QTM} / s	Effect	Ref.
CoCP		0.045		1.1(8) x 10^3	0.9(2)	6.0(1)	-	QTM	This
		0.1		0.9(4) x 10^3	0.9(2)	6.0(1)	-	Direct	work
		0.3		0.5(3) x 10^{-2}	0.9(2)	6.0(1)	3(1)x10^3	Raman	
cis-[Co(hfac)$_2$(H_2O)$_2$]		0.1		7225.7	106.4	4.9		Direct Raman	1
[Co(dca)$_2$(bim)$_4$]	0.87 x 10^{-6}	0.25	7.74					Orbach	2
[Co(dca)$_2$(bim)$_2$]$_n$	1.54 x 10^{-6}	0.25	5.33					Orbach	2
[Co(dca)$_2$(bmim)$_2$]$_n$	0.63 x 10^{-6}	0.25	13.81					Orbach	2
[Co(dca)$_2$(atz)$_2$]$_n$	1.7 x 10^{-6}	0.1	5.1					Orbach	3
[Co(ppad)$_2$]$_n$	5.03 x 10^{-6}	0.2	11.37					Orbach	4
[Co(AcO)$_2$(py)$_2$(H_2O)$_2$]	6.7 x 10^{-7}	0.15	25.0				0.011	Orbach	5
[Co(pydm)$_2$](dnbz)$_2$]	2. 8(4) x 10^{-9}[(a)]	0.2	44.1(8)[(a)]		72(28)[(a)]	2.3[(a)]		QTM Raman Orbach	6
(NBu_4)[Co(piv)$_3$]		0.1			0.19	8.3		Raman	7

Abbreviations: hfac = hexafluoroacetylacetonate; dca = dicyanamide; bim = 1-benzylimidazole; bmim = 1-benzyl-2-methylimidazole; atz = 2-amino-1,3,5-triazine; ppad = N3-(3-pyridoyl)-3-pyridinecarboxamidrazone; AcO = acetate anion; py = pyridyl; pydm = 2,6-pyridinedimethanol; dnbz = 3,5-dinitrobenzoato(1-); ac = acetato; Melm = 1-methylimidazole; piv = pivalato

References

(1) Korchagin, D. V.; Palii, A. V.; Yureva, E. A.; Akimov, A. V.; Misochko, E. Y.; Shilov, G. V.; Talantsev, A. D.; Morgunov, R. B.; Shakin, A. A.; Aldoshin, S. M.; Tsukerblat, B. S. Evidence of Field Induced Slow Magnetic Relaxation in Cis-[Co(Hfac) 2 (H 2 O) 2] Exhibiting Tri-Axial Anisotropy with a Negative Axial Component. *Dalt. Trans.* **2017**, *46*, 7540–7548.

(2) Anna Świtlicka-Olszewska, J. P.-G.; Klemens, T.; Machura, B.; Vallejo, J.; Cano, J.; Lloretb, F.; Julve, M. Dalton Transactions. *Dalt. Trans.* **2016**, *45* (25), 10181–10193.

(3) Palion-gazda, J.; Klemens, T.; Machura, B.; Vallejo, J.; Lloret, F.; Julve, M. Single Ion Magnet Behaviour in a Two-Dimensional Network of Dicyanamide-Bridged Cobalt(II) Ions. *Dalt. Trans.* **2015**, *44* (7), 2989–2992.

(4) Liu, X.; Sun, L.; Zhou, H.; Cen, P.; Jin, X.; Xie, G.; Chen, S.; Hu, Q. Single-Ion-Magnet Behavior in a Two-Dimensional Coordination Polymer Constructed from Co. *Inorg. Chem.* **2015**, *54* (18), 8884–8886.

(5) Walsh, J. P. S.; Bowling, G.; Ariciu, A.; Jailani, N. F. M.; Chilton, N. F.; Waddell, P. G.; Collison, D.; Tuna, F.; Higham, L. J. Evidence of Slow Magnetic Relaxation in Co(AcO)2 (Py)2(H2O)2. *Magnetochemistry* **2016**, *2* (2), 23–33.

(6) Valigura, D.; Rajnák, C.; Moncol, J.; Titiš, J.; Boča, R. A Mononuclear Co(II) Complex Formed from Pyridinedimethanol with Manifold Slow Relaxation Channels. *Dalt. Trans.* **2017**, *46* (33), 10950–10956.

(7) Chen, S.-Y.; Hui-Hui Cui, Y.-Q. Z.; Wang, Z.; Ouyang, Z.-W.; Chen, L.; Chen, X.-T.; Hong Yan, A.; Xue, Z.-L. Magnetic Anisotropy and Relaxation Behavior of Six-Coordinate Tris(Pivalato)-Co(II) and -Ni(II) Complexes Shu-Yang. *Dalt. Trans.* **2018**, *47* (30), 10162–10171.